NJC

Accepted Manuscript

This is an *Accepted Manuscript*, which has been through the Royal Society of Chemistry peer review process and has been accepted for publication.

Accepted Manuscripts are published online shortly after acceptance, before technical editing, formatting and proof reading. Using this free service, authors can make their results available to the community, in citable form, before we publish the edited article. We will replace this *Accepted Manuscript* with the edited and formatted *Advance Article* as soon as it is available.

You can find more information about *Accepted Manuscripts* in the Information for Authors.

Please note that technical editing may introduce minor changes to the text and/or graphics, which may alter content. The journal's standard Terms & Conditions and the Ethical guidelines still apply. In no event shall the Royal Society of Chemistry be held responsible for any errors or omissions in this *Accepted Manuscript* or any consequences arising from the use of any information it contains.

ROYAL SOCIETY OF CHEMISTRY

www.rsc.org/njc

Ultrathin Porous Hierarchically Textured $NiCo_2O_4$/Graphene Oxide Flexible Nanosheets for High-Performance Supercapacitors

Elias Mitchell[a], Ashley Jimenez[a], Ram K. Gupta[a*], Bipin Kumar Gupta[b], Karthik Ramasamy[c], Mohammad Shahabuddin[d], Sanjay R. Mishra[d]

[a]Department of Chemistry, Pittsburg State University, 1701 S. Broadway, Pittsburg, KS 66762, USA

[b]National Physical Laboratory (CSIR), Dr K.S. Krishnan Road, New Delhi 110012, India

[c]The Center for Integrated Nanotechnologies, Los Alamos National Laboratory, Albuquerque, NM 87545, USA

[d]Department of Physics, The University of Memphis, Memphis, TN 38152, USA

Abstract:

The ultimate goal of supercapacitor research industries is to develop devices which could be used as flexible, portable, ultrathin and highly-efficient power sources. However, the bulk $NiCo_2O_4$ materials prevents the achievement of high energy density as well as immense rate performance due to the limited electroactive surface area. In this work, we proposed a new breakthrough strategy to develop a highly porous hierarchical flexible nanosheets of $NiCo_2O_4$-graphene oxide ($NiCo_2O_4$-GO) on nickel foam by a facile electrochemical deposition method. The morphogenesis of $NiCo_2O_4$-GO hybrid nanostructure based electrode exhibit hierarchical porous flexible nanosheets like structures. The electrochemical properties of these electrodes were investigated by cyclic voltammetry and galvanostatic charge-discharge measurements in 3M KOH electrolyte. The obtained results exhibit that this new hybrid nanostructure has a specific capacitance of 1078 F/g at a discharge current of 1 mA with great cyclic stability. These excellent capacitive performances of $NiCo_2O_4$-GO can be attributed due to its hierarchical porous nanosheets like unique structure. This unique structure provides efficient ion transport that is highly desirable for superior rate capability and excellent cycling stability. Hence, our method provides a promising facile and binder free nanostructure electrodes for next generation high-performance supercapacitor applications.

KEYWORDS: $NiCo_2O_4$, graphene oxide, cyclic voltammetry, supercapacitor, cyclic stability

* Corresponding author. Tel.: +1 620 2354763; fax: +1 620 2354003
E-mail address: ramguptamsu@gmail.com(R.K. Gupta).

INTRODUCTION

To solve the increasing demand for energy, it is perfect time for the researchers to develop sustainable and reproducible energy system. Recently, tremendous efforts have been devoted to build up more efficient energy production and storage devices to solve global energy problems.[1-7] Among various devices, supercapacitors are emerging as a novel technology to store energy efficiently due to their high power densities, fast charge-discharge capabilities and long cycle lives.[8-11] These unique properties make them very expedient for the applications in emergency power systems, electric vehicles, and devices where high-power delivery is required.[12-15] The charge storage mechanism of a supercapacitor can be divided into two groups: (i) electrical double-layer capacitors (EDLCs) where the charge is stored at the interface between the electrode and the electrolyte, and (ii) redox electrochemical capacitors (pseudocapacitors), in which charge storage arises due to Faradaic reactions at electrode/electrolyte interface.[16] In terms of charge storage capacity, pseudocapacitors are much better than EDLSCs but suffer from high cost and poor cyclic stability arising from the low conductivity of the active materials.[14] Pseudocapacitors are usually made-up of using transition metal oxides, hydroxides and conducting polymers whereas, EDLCs are made-up of using carbon based materials.[17, 18] The performance of a pseudocapacitor can be improved by developing a hybrid nanostructured material associated with metal oxide and carbon based material.[19, 20]

Till date, several promising materials, including nickel oxide, ruthenium oxide, cobalt oxide, iron oxide and manganese oxide, have been studied as electrode materials for supercapacitor applications.[21-30] However, most of these materials often suffer from low capacitance and/or poor cycling stability due to large volume change during charge-discharge process.[31] This problem could be addressed by developing a hybrid porous nanostructured material which contains

carbon and metal oxide.[32, 33] The porous structure could accommodate the large volume change due to insertion and removal of electrolyte ions during charge-discharge process. Among the carbon based materials, graphene oxide is very attractive due to its unique properties such as high conductivity, good mechanical flexibility, large theoretical surface area (2630 m^2/g), high thermal and chemical stability.[34, 35] On the other hand, $NiCo_2O_4$ is a promising material for the pseudocapacitors due to its higher charge storage capacity (theoretical capacitance: 3560 F/g) and relatively low cost compare to other oxides.[36-40] The performance of a hybrid nanostructured material as an electrode for supercapacitor could be further improved by directly growing on conductive substrates.[41] By growing on conductive substrates, each nanostructure gets its own electric contact with the substrate. Thus, it can be participate in the electrochemical reactions.

Recently, Zhang et. al. have deposited single-crystalline nano-needle arrays of $NiCo_2O_4$ on Ni foam and Ti foil through a solution method.[42] The specific capacitance of $NiCo_2O_4$ nano-needle arrays was estimated to be 1118.6 F/g. This specific capacitance of $NiCo_2O_4$ nano-needle grown on metallic substrate was much higher than that of free-standing porous $NiCo_2O_4$ nanowires. Furthermore, Yang et. al. have fabricated nanostructured porous MnO_2 film on Ni foam via a cyclic voltammetry electrodeposition method.[43] They reported a maximum specific capacitance of 2790 mF/cm^2 at 2 mA/cm^2 and 864 mF/cm^2 at 20 mA/cm^2. Nanostructured $NiCo_2O_4$ with different morphologies were directly grown on the conductive substrates (stainless steel and ITO) by an electrodeposition method.[44] The stainless steel substrate supported $NiCo_2O_4$ was successfully used as an electrode for methanol oxidation and exhibited high electro-catalytic activity. Liu et. al. have fabricated hierarchical $NiCo_2O_4$@$NiCo_2O_4$ core/shell nano-flake arrays on nickel foam for high-performance supercapacitors.[45] It was reported that compared with the bare $NiCo_2O_4$ nano-flake arrays, the core/shell electrode displays better pseudocapacitive

behaviors. The specific capacitance was observed to be 2.20 F/cm^2 at a current density of 5 mA/cm^2. The enhanced pseudocapacitive performances were achieved due to the unique core/shell structure, which provides fast ion and electron transfer and a large number of active sites for electrochemical reactions.

Here in this report, a hierarchical porous $NiCo_2O_4$/Graphene oxide hybrid flexible nanostructure sheets has been fabricated via a simple electrodeposition method followed by heat treatment. The hierarchical porous $NiCo_2O_4$/Graphene oxide hybrid flexible nanostructure sheets has been fully characterized in terms of gross structure and surface morphogenesis by XRD, Raman, FT-IR and scanning electron microscopy techniques. The results obtained from the cyclic voltammetry and galvanostatic charge-discharge tests revealed that the $NiCo_2O_4$-GO electrode possessed very high specific capacitances of 1078 F/g with excellent cyclic stability which legitimates its potential use in supercapacitor applications.

METHODS

Synthesis of Ni foam supported $NiCo_2O_4$ and $NiCo_2O_4$-GO

$Ni(NO_3)_2.6H_2O$ and $Co(NO_3)_2.6H_2O$ of analytical grade were used in experiments without further purification. Graphene oxide was synthesized by the modified Hummer's method described in our previous publication.[46] Before electrodeposition, the nickel foam was cleaned with 3M HCl solution in an ultrasound bath for 20 min in order to remove the NiO layer on the surface, and then rinsed with de-ionized water and absolute ethanol. The electrodeposition has been performed in a standard three-electrode cell using Ni foam as a working electrode. Electrodeposition was carried out using VersaSTAT 4 (Princeton Applied Research) in 20 ml DI water having 1 mmol of $Ni(NO_3)_2.6H_2O$ and 2 mmol of $Co(NO_3)_2.6H_2O$. The electrodeposition

potential was -1.0 V (vs. Ag/AgCl electrode). After electro-deposition for 2000 sec, the Ni foam was rinsed several times with de-ionized water and absolute ethanol. After washing, the nickel foam was calcined at 350 °C for 3 h. Similar method was adopted for $NiCo_2O_4$-GO deposition except the solution contains 20 mg of water dispersed GO. The GO was dispersed using ultrasonication for 20 min to make homogeneous dispersed solution.

Instrumentation and sample analysis

The structural characterization and surface morphology of the $NiCo_2O_4$-GO hybrid nanostructure was performed using X-ray diffraction (XRD), FT-IR spectroscopy, scanning electron microscopy (SEM) and Raman spectroscopy. The XRD spectra was recorded with Shimadzu X-ray diffractometer using the 2θ-θ scan with $CuK_{\alpha 1}$ (λ=1.5406 Å) radiation. The FT-IR spectrum was recorded on a Shimadzu IR Affinity-1. A Philips XL 30 environmental scanning electron microscope (SEM) was used to record the microstructure of the materials. The Raman spectrum was recorded at room-temperature using a Renishaw 1000 micro-Raman system equipped with a Leica microscope. The 50×- magnifying objective of the microscope focused a laser beam to a spot of ~1 μm diameter. The excitation wavelength used was 514.5 nm from an Ar^+ ion laser and 1800 line/mm grating was used in all measurements, which allowed one to obtain a resolution of ~1 cm^{-1}.

Electrochemical measurements

The electrochemical measurements were performed in a standard three electrode cell containing a platinum wire as a counter electrode, saturated calomel electrode (SCE) as a reference electrode, and $NiCo_2O_4$ and $NiCo_2O_4$-GO deposited Ni foam as a working electrode.

The loading mass of $NiCo_2O_4$ and $NiCo_2O_4$-GO on nickel foam after electrodeposition and heat treatment was about 1 mg. The deposited weight after electrodeposition was accurately measured by weighing the nickel foam before and after deposition, drying and heating with an analytical balance (model MS105DU, Mettler Toledo, max. 120g, 0.01mg of resolution). An aqueous solution containing 3M KOH was used as an electrolyte. The supercapacitive performance was evaluated by cyclic voltammetry (CV) and galvanostatic charge-discharge techniques. Electrochemical measurements were performed on a VersaSTAT 4-500 electrochemical workstation (Princeton Applied Research, USA).

RESULTS AND DISCUSSION

Nanostructured $NiCo_2O_4$ and $NiCo_2O_4$-GO were electrodeposited on the nickel foam using nitrate salts of nickel and cobalt. During the electrodeposition, following reaction occurs at the Ni foam:

$$NO_3^- + 7H_2O + 8e^- \rightarrow NH_4^+ + 10OH^- \quad \text{..... (1)}$$

$$Ni^{2+} + 2Co^{2+} + 6OH^- \rightarrow NiCo_2(OH)_6 \quad \text{..... (2)}$$

The mixed metal hydroxide precursor converted to $NiCo_2O_4$ upon calcination

$$NiCo_2(OH)_6 + \frac{1}{2}O_2 \rightarrow NiCo_2O_4 + 3H_2O \quad \text{..... (3)}$$

The synthesized materials and the electrodes were structurally and electrochemically characterized for their applications as an electrode for supercapacitors. In the subsequent sections, we present details of the results and discussion.

The X-ray diffraction pattern of synthesized graphene oxide (Figure S1; see supporting information) shows a broad peak near 10.63°. This peak of the graphene oxide corresponds to the interlayer spacing of 8.32 Å. There was no peak around 10.63° in the graphite which was the

starting material for this synthesis. The appearance of (002) peak at 10.63° indicates that oxygenated groups and H_2O molecules have been inserted in the interlayer of the graphite which causes increase in the interlayer spacing.[47] The FT-IR spectrum of the graphene oxide shows (Figure S2; see supporting information) a peak at 1734 cm^{-1} which corresponds to the C=O stretching mode of carboxylic group on the graphene oxide.[48] The other peaks at 1102 cm^{-1} and 1622 cm^{-1} correspond to the alkoxy C-O stretching vibration and the C-O stretch mode of the carboxylic groups.[49] The broad absorption peak in the range of 3300-3500 cm^{-1} is due to O-H stretching vibration arising from hydroxyl groups. The Raman spectrum of the graphene oxide shows the characteristics D and G band of the carbon (Figure S3; see supporting information). These structural analyses have confirmed the formation of high quality graphene oxide.

The X-ray diffraction pattern of the $NiCo_2O_4$ grown on nickel foam is shown in Figure 1. Apart from the peaks due to nickel foam, all the peaks correspond to $NiCo_2O_4$ crystalline structure. The peaks at 31.2°, 36.7°, 56°, 59.1° and 64.9° have indexed to (220), (311), (422), (511) and (440) plane reflections of the spinel $NiCo_2O_4$ (JCPDF file no. 20-0781; space group: $F*3$(202)). The absence of any peaks other than due to $NiCo_2O_4$ and nickel foam suggests phase purity of the electrodeposited $NiCo_2O_4$. We did not observe any peaks related to graphene oxide in the XRD patterns of $NiCo_2O_4$-GO which could be due to high intensity of nickel foam and $NiCo_2O_4$. SEM images of the $NiCo_2O_4$ and $NiCo_2O_4$-GO coated nickel foam are shown in Figure 2a-d. As seen in the SEM images, the morphology of the $NiCo_2O_4$ changes drastically by incorporation of graphene oxide in the electrolyte during electrode position of $NiCo_2O_4$. The higher magnification images of $NiCo_2O_4$-GO (Figure 2c,d) shows hierarchical nanosheet like structures having higher porosity through the surface of the sample. The size of these sheets are about 1 μm by 1 μm with thickness of only few nanometers. These nanosheets with high surface

area in addition to Faradic charge storage due to $NiCo_2O_4$ could be very suitable for fabrication of high performance pseudocapacitors.

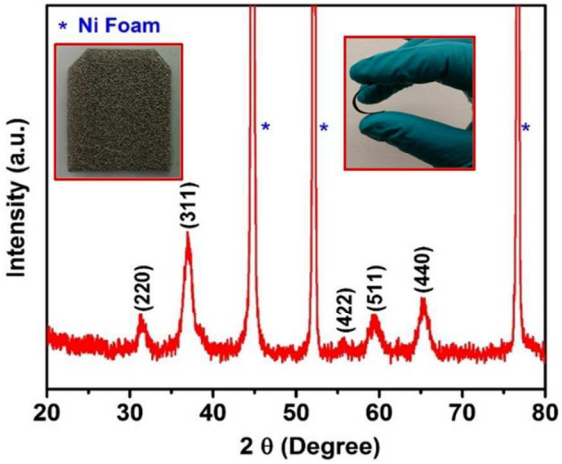

Figure 1: XRD patterns of $NiCo_2O_4$ on Ni foam (the inset figure shows (left) the digital image of Ni foam and (right) flexibility of the electrode).

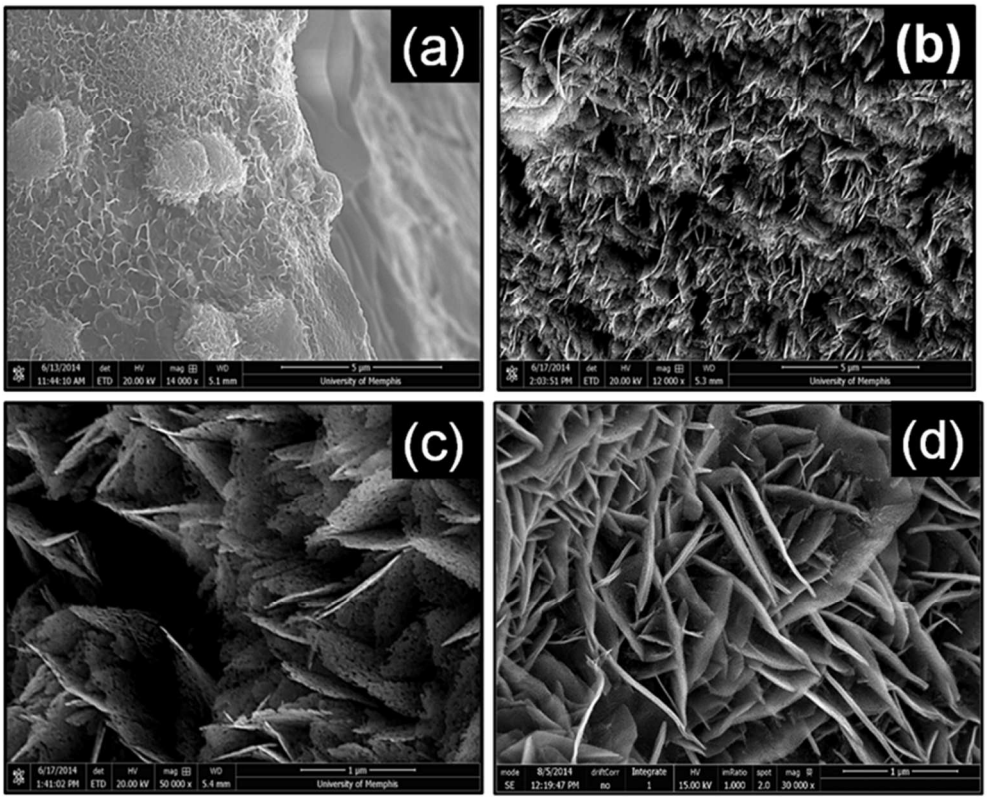

Figure 2: SEM images of (a) $NiCo_2O_4$, (b) $NiCo_2O_4$-GO, (c) higher magnification of $NiCo_2O_4$-GO (top view), and (d) higher magnification of $NiCo_2O_4$-GO (angle view).

Electrochemical measurements were performed to evaluate the potential application of these materials as an electrode for supercapacitors. Figure 3 shows the cyclic voltammetry (CV) curves of $NiCo_2O_4$ and $NiCo_2O_4$-GO electrodes at various scan rates. As seen in the CV curves, a pair of redox (anodic and cathodic) peaks were observed. These redox peaks in the alkaline electrolyte are due to the M-O/M-O-OH (where M= Ni, Co) conversion.[50] The CV curves of the $NiCo_2O_4$ and $NiCo_2O_4$-GO electrodes at various scan rate shows that the peak current increases with increase in the scan rate and difference in the cathodic and anodic peak potential expands gradually. The peak current increases linearly with the increasing of square root of scan rates (Figure S4; see supporting information) indicating that the reaction kinetics followed during the redox reactions may be controlled by diffusion process.[51] Compared with $NiCo_2O_4$, the higher peak current density of $NiCo_2O_4$-GO is an indication of better charge transfer which could be due to graphene's higher electrical conductivity and larger surface area with good porosity of $NiCo_2O_4$-GO electrode. The long term cyclic stability of $NiCo_2O_4$-GO electrode was also investigated using cyclic voltammetry. Figure 4 shows the CV curves of $NiCo_2O_4$-GO electrode at various cycles. As seen in the CV curves, the shape and area of the voltammograms nearly appear identical, suggesting high cyclic stability of the $NiCo_2O_4$-GO electrode.

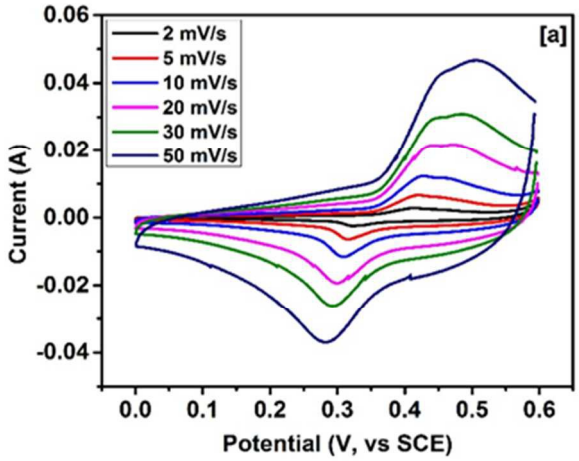

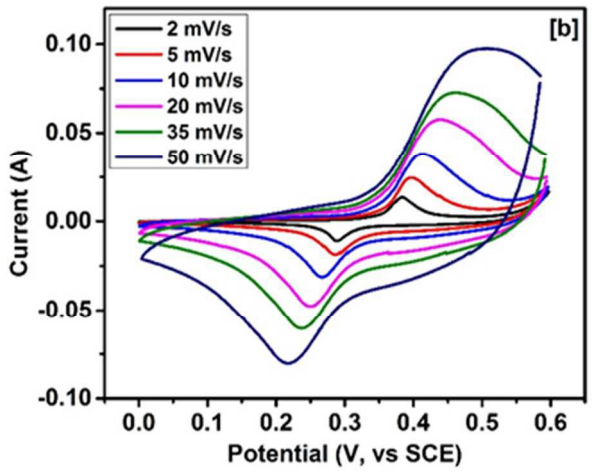

Figure 3: CV curves of (a) $NiCo_2O_4$ and (b) $NiCo_2O_4$-GO at various scan rates.

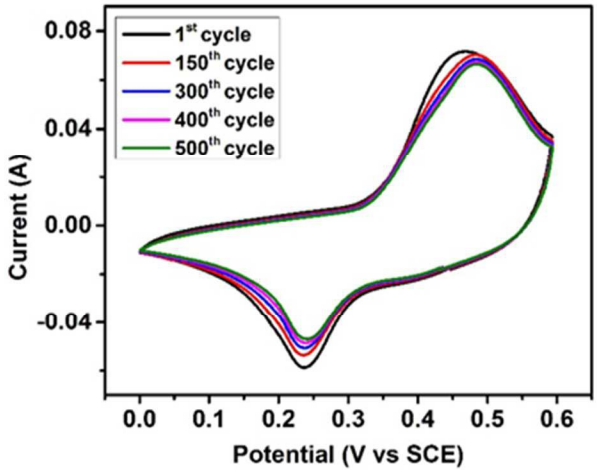

Figure 4: CV curves of $NiCo_2O_4$-GO at various number of cycles.

The applicability of the $NiCo_2O_4$-GO electrode for flexible charge storage device was investigated by measuring the change in electrical resistivity as a function of bending angles. As seen in Figure 5, apparently there is no change in the electrical resistivity of the $NiCo_2O_4$-GO electrode on bending from 0 to 170^o. As seen in the inset of Figure 5, $NiCo_2O_4$-GO electrode shows high degree of flexibility without degrading its properties. In addition, the CV curves of $NiCo_2O_4$-GO electrode at various angles of bending show identical shape (inset of Figure 5),

indicating electrochemical stability of the electrode on bending. Almost similar electrical and charge storage properties of $NiCo_2O_4$-GO electrode at various bending angles suggest that it can be successfully used as an electrode for flexible charge storage devices.

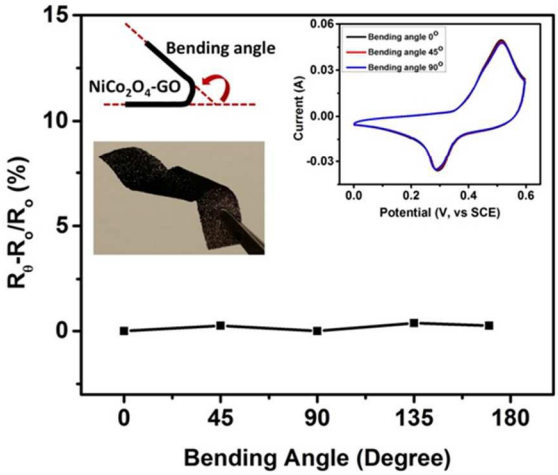

Figure 5: Electrical-resistance variation of $NiCo_2O_4$-GO electrode vs. different bending angles. Inset shows the digital photographs of bended electrode and CV curves at various angles of bending.

In order to probe the suitability and cyclic stability of the electrodes for supercapacitor applications, the constant current charge-discharge measurement was carried out. Figure 6 shows the discharge curve of $NiCo_2O_4$ and $NiCo_2O_4$-GO at various applied current in the potential range of 0-0.4V. The specific capacitance (C_{sp}) of the electrode was calculated according to the following equation[52]

$$C_{sp} = \frac{I \times \Delta t}{\Delta V \times m} \qquad \text{..... (4)}$$

Where, I is the discharge current (A), Δt is the discharge time (s), ΔV is the potential window (V), and m is the mass (g) of the active material. Figure 7 shows the variation of specific capacitance versus applied current for $NiCo_2O_4$ and $NiCo_2O_4$-GO electrodes. The specific capacitance of $NiCo_2O_4$-GO electrode was 1078 and 999 F/g at the current of 1 and 5 mA, respectively. Such a large value of specific capacitance can be attributed to the unique porous and nanosheets like

structure of $NiCo_2O_4$-GO. As seen in the Figure 7, there is a decrease in the specific capacitance with increasing current. The decrease in the specific capacitance with the increase of the discharge current is likely caused by the increase of potential drop and insufficient faradic redox reaction of the $NiCo_2O_4$ under higher discharge currents.[53] Table 1 shows the specific capacitance of $NiCo_2O_4$ and $NiCo_2O_4$-GO synthesized in this work and other studies.

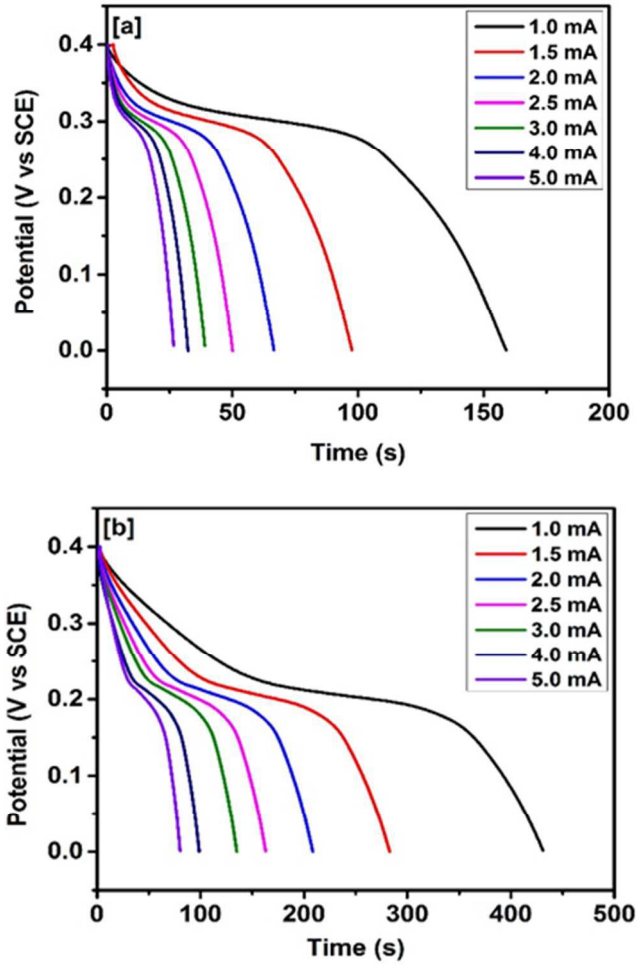

Figure 6: Galvanic discharge characteristics of (a) $NiCo_2O_4$ and (b) $NiCo_2O_4$-GO at various discharge currents.

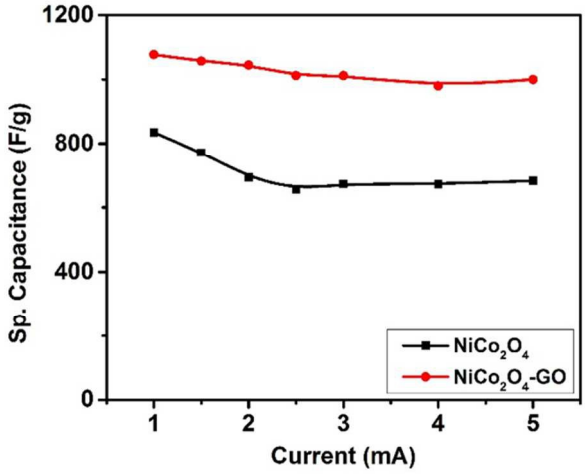

Figure 7: Specific capacitance versus current for (a) $NiCo_2O_4$ and (b) $NiCo_2O_4$-GO.

Table 1: Specific capacitance of the $NiCo_2O_4$ based materials prepared in present work and other reports in previous works.

Sample	Specific Capacitance (F/g)	Preparation method[Ref]
$NiCo_2O_4$ nanoneedles	1119	solution[42]
$NiCo_2O_4$ film	490	chemical bath deposition[54]
$NiCo_2O_4$ film	580	electrochemical[55]
$NiCo_2O_4$ flowerlike	658	hydrothermal[56]
$NiCo_2O_4$-rGO nanoflake	1693	solution[57]
$NiCo_2O_4$ mesoporous spinel	764	solution[58]
$NiCo_2O_4$-rGO nanoplates	947	hydrothermal[59]
$NiCo_2O_4$-nitrogen doped GO nanowires	1273	hydrothermal[60]
$NiCo_2O_4$ nanoparticles	671	co-precipitation[61]
NiCo2O4 nanocrystals	580	electrochemical[55]
NiCo2O4 crystals	217	Sol-gel[62]
$NiCo_2O_4$-rGO nanowires	737	hydrothermal[63]
$NiCo_2O_4$	835	electrochemical (this work)
$NiCo_2O_4$-GO	1078	electrochemical (this work)

Figure 8 shows the change in the specific capacitance of the $NiCo_2O_4$-GO electrode measured for 1000 charge/discharge cycles. The inset of Figure 8 shows first few cycles of charge-discharge curves. It is seen that the capacitance of the electrode first underwent a gradual decrease followed by constant capacitance retention. The electrochemical studies show that

$NiCo_2O_4$-GO electrode has considerably higher specific capacitance than $NiCo_2O_4$ electrode. This could be due to fact that the specific capacitance of $NiCo_2O_4$-GO electrode is improved by having porous and nanosheet like structure as evidenced by the SEM images (Figure 2). The porous and nanosheet structured $NiCo_2O_4$-GO electrode provides higher specific surface area, which leads to the enhanced liquid-solid interfacial area for the insertion/extraction of electrolyte ions. In addition to porous and nanosheet like structure of the $NiCo_2O_4$-GO electrode, $NiCo_2O_4$ participate in the redox capacitive mechanisms which further improve the charge storage capacity. This unique structure allows to fast access of the electrolytes to the larger surface of $NiCo_2O_4$-GO and thus results in a low ion-transport resistance. This is further supported by excellent rate capability of the $NiCo_2O_4$-GO electrode even at higher discharge current. The obtained excellent results fully justify its potential applications in proposed next generation flexible supercapacitors.

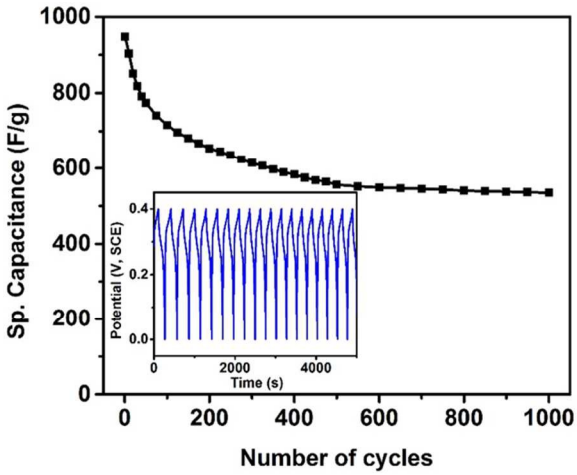

Figure 8: Cycling performance of $NiCo_2O_4$-GO electrode at constant current of 3mA. The inset shows the first few cycles of charge-discharge curves.

CONCLUSIONS

In conclusion, we have proposed the first hierarchical porous $NiCo_2O_4$/Graphene oxide hybrid flexible nanostructure sheets electrodes for next generation supercapacitors using a facile

electrochemical deposition technique. The nanostructured $NiCo_2O_4$-GO shows excellent specific capacitance of 1078 F/g at a discharge current of 1 mA with a great cyclic stability. The excellent electrochemical performances of $NiCo_2O_4$-GO electrode are related to its unique porous and nanosheet like structure. The nanosheet structure greatly enhances the active sites for the Faradic redox reaction of $NiCo_2O_4$, while the porous structure provides large accessible surface area for enhanced charge storage. Thus, we envision that the flexible binder free electrodes with high specific capacitance would be a key to developing supercapacitor devices that can readily be incorporated for practical applications.

Conflict of Interest: The authors declare no competing financial interest.

Acknowledgment. Authors wish to thank Pittsburg State University for providing financial support. Authors also wish to thank Integrated Microscopy Center at the University of Memphis for providing FE-SEM facility.

Supporting Information Available: Additional experimental data. This material is available free of charge *via* the Internet.

REFERENCES AND NOTES

1. N. Ashok Kumar and J.-B. Baek, *Chem. Commun.*, 2014, **50**, 6298-6308.
2. Z.-S. Wu, G. Zhou, L.-C. Yin, W. Ren, F. Li and H.-M. Cheng, *Nano Energy*, 2012, **1**, 107-131.
3. G. Yu, X. Xie, L. Pan, Z. Bao and Y. Cui, *Nano Energy*, 2013, **2**, 213-234.
4. C. Xiao, X. Yu, D. Yang and D. Que, *Sol. Energy Mater. Sol. Cells*, 2014, **128**, 427-434.
5. A. Majkić, C. Gadermaier, N. Celic, P. Topolovsek, G. Bratina and D. Mihailovic, *Sol. Energy Mater. Sol. Cells*, 2014, **127**, 63-66.
6. V. J. Babu, S. Vempati, S. Sundarrajan, M. Sireesha and S. Ramakrishna, *Solar Energy*, 2014, **106**, 1-22.
7. H. Pang, C. Wei, X. Li, G. Li, Y. Ma, S. Li, J. Chen and J. Zhang, *Sci. Rep.*, 2014, **4**, 3577.
8. P. Zhao, W. Li, G. Wang, B. Yu, X. Li, J. Bai and Z. Ren, *J. Alloys Compd.*, 2014, **604**, 87-93.
9. R. Vellacheri, A. Al-Haddad, H. Zhao, W. Wang, C. Wang and Y. Lei, *Nano Energy*, 2014, **8**, 231-237.
10. C. Ma, Y. Li, J. Shi, Y. Song and L. Liu, *Chem Eng J*, 2014, **249**, 216-225.
11. C. Zhang, H. Yin, M. Han, Z. Dai, H. Pang, Y. Zheng, Y.-Q. Lan, J. Bao and J. Zhu, *ACS Nano*, 2014, **8**, 3761-3770.
12. F. Zhao, Y. Wang, X. Xu, Y. Liu, R. Song, G. Lu and Y. Li, *ACS Applied Materials & Interfaces*, 2014, **6**, 11007-11012.
13. G. Wang, L. Zhang and J. Zhang, *Chem Soc Rev*, 2012, **41**, 797-828.
14. P. Simon and Y. Gogotsi, *Nat Mater*, 2008, **7**, 845-854.
15. R. Kötz and M. Carlen, *Electrochim. Acta*, 2000, **45**, 2483-2498.
16. M. Winter and R. J. Brodd, *Chem. Rev.*, 2004, **104**, 4245-4270.
17. W. Yang, Z. Gao, J. Ma, J. Wang, B. Wang and L. Liu, *Electrochim. Acta*, 2013, **112**, 378-385.
18. M. Nasibi, M. A. Golozar and G. Rashed, *Mater. Lett.*, 2013, **91**, 323-325.
19. Q. Li, X. Hu, Q. Yang, Z. Yan, L. Kang, Z. Lei, Z. Yang and Z. Liu, *Electrochim. Acta*, 2014, **119**, 184-191.
20. S. Yang, X. Song, P. Zhang and L. Gao, *ACS Applied Materials & Interfaces*, 2013, **5**, 3317-3322.
21. X. Yan, X. Tong, J. Wang, C. Gong, M. Zhang and L. Liang, *J. Alloys Compd.*, 2014, **593**, 184-189.
22. B. Ren, M. Fan, Q. Liu, J. Wang, D. Song and X. Bai, *Electrochim. Acta*, 2013, **92**, 197-204.
23. J. Xu, L. Gao, J. Cao, W. Wang and Z. Chen, *Electrochim. Acta*, 2010, **56**, 732-736.
24. J. H. Kwak, Y.-W. Lee and J. H. Bang, *Mater. Lett.*, 2013, **110**, 237-240.
25. L. Wang, X. Zhang, S. Wang, Y. Li, B. Qian, X. Jiang and G. Yang, *Powder Technol.*, 2014, **256**, 499-505.
26. J. Chen, K. Huang and S. Liu, *Electrochim. Acta*, 2009, **55**, 1-5.
27. Y. Zhao, Y. Meng and P. Jiang, *J. Power Sources*, 2014, **259**, 219-226.
28. Y. Zhao and P. Jiang, *Colloids and Surfaces A: Physicochemical and Engineering Aspects*, 2014, **444**, 232-239.
29. Z. Chen, J. Li, Y. Chen, Y. Zhang, G. Xu, J. Yang and Y. Feng, *Particuology*, 2014, **15**, 27-33.
30. E. Mitchell, R. K. Gupta, K. Mensah-Darkwa, D. Kumar, K. Ramasamy, B. K. Gupta and P. Kahol, *New J. Chem.*, 2014, **38**, 4344-4350.
31. S. Park and S. Kim, *Electrochim. Acta*, 2013, **89**, 516-522.
32. K. Naoi, *Fuel Cells*, 2010, **10**, 825-833.
33. H.-W. Wang, Z.-A. Hu, Y.-Q. Chang, Y.-L. Chen, Z.-Y. Zhang, Y.-Y. Yang and H.-Y. Wu, *Mater. Chem. Phys.*, 2011, **130**, 672-679.

34. X. Jiang, Y. Ma, J. Li, Q. Fan and W. Huang, *The Journal of Physical Chemistry C*, 2010, **114**, 22462-22465.
35. H. M. Jeong, J. W. Lee, W. H. Shin, Y. J. Choi, H. J. Shin, J. K. Kang and J. W. Choi, *Nano Lett.*, 2011, **11**, 2472-2477.
36. M.-T. Lee, J.-K. Chang, Y.-T. Hsieh and W.-T. Tsai, *J. Power Sources*, 2008, **185**, 1550-1556.
37. T.-Y. Wei, C.-H. Chen, H.-C. Chien, S.-Y. Lu and C.-C. Hu, *Advanced Materials*, 2010, **22**, 347-351.
38. H. Wang, Q. Gao and L. Jiang, *Small*, 2011, **7**, 2454-2459.
39. H. B. Wu, H. Pang and X. W. Lou, *Energy & Environmental Science*, 2013, **6**, 3619-3626.
40. Y. Li, Y. Zhang, Y. Li, Z. Wang, H. Fu, X. Zhang, Y. Chen, H. Zhang and X. Li, *Electrochim. Acta*, 2014, **145**, 177-184.
41. Y. Gao, S. Chen, D. Cao, G. Wang and J. Yin, *J. Power Sources*, 2010, **195**, 1757-1760.
42. G. Q. Zhang, H. B. Wu, H. E. Hoster, M. B. Chan-Park and X. W. Lou, *Energy & Environmental Science*, 2012, **5**, 9453-9456.
43. J. Yang, L. Lian, H. Ruan, F. Xie and M. Wei, *Electrochim. Acta*, 2014, **136**, 189-194.
44. L. Qian, L. Gu, L. Yang, H. Yuan and D. Xiao, *Nanoscale*, 2013, **5**, 7388-7396.
45. X. Liu, S. Shi, Q. Xiong, L. Li, Y. Zhang, H. Tang, C. Gu, X. Wang and J. Tu, *ACS Applied Materials & Interfaces*, 2013, **5**, 8790-8795.
46. A. A. Al-Ghamdi, R. K. Gupta, P. K. Kahol, S. Wageh, Y. A. Al-Turki, W. El Shirbeeny and F. Yakuphanoglu, *Solid State Commun.*, 2014, **183**, 56-59.
47. Y. Bai, R. B. Rakhi, W. Chen and H. N. Alshareef, *J. Power Sources*, 2013, **233**, 313-319.
48. J.-D. Qiu, J. Huang and R.-P. Liang, *Sensors and Actuators B: Chemical*, 2011, **160**, 287-294.
49. C. Xu, J. Li, X. Wang, J. Wang, L. Wan, Y. Li, M. Zhang, X. Shang and Y. Yang, *Mater. Chem. Phys.*, 2012, **132**, 858-864.
50. X. Y. Liu, Y. Q. Zhang, X. H. Xia, S. J. Shi, Y. Lu, X. L. Wang, C. D. Gu and J. P. Tu, *J. Power Sources*, 2013, **239**, 157-163.
51. R. Tummala, R. K. Guduru and P. S. Mohanty, *J. Power Sources*, 2012, **209**, 44-51.
52. J. Gomez and E. E. Kalu, *J. Power Sources*, 2013, **230**, 218-224.
53. X. Qing, S. Liu, K. Huang, K. Lv, Y. Yang, Z. Lu, D. Fang and X. Liang, *Electrochim. Acta*, 2011, **56**, 4985-4991.
54. R. R. Salunkhe, K. Jang, H. Yu, S. Yu, T. Ganesh, S.-H. Han and H. Ahn, *J. Alloys Compd.*, 2011, **509**, 6677-6682.
55. V. Gupta, S. Gupta and N. Miura, *J. Power Sources*, 2010, **195**, 3757-3760.
56. H. Chen, J. Jiang, L. Zhang, T. Qi, D. Xia and H. Wan, *J. Power Sources*, 2014, **248**, 28-36.
57. L. Wang, X. Wang, X. Xiao, F. Xu, Y. Sun and Z. Li, *Electrochim. Acta*, 2013, **111**, 937-945.
58. C.-T. Hsu and C.-C. Hu, *J. Power Sources*, 2013, **242**, 662-671.
59. L. Ma, X. Shen, H. Zhou, Z. Ji, K. Chen and G. Zhu, *Chem Eng J*, 2015, **262**, 980-988.
60. M. Yu, J. Chen, Y. Ma, J. Zhang, J. Liu, S. Li and J. An, *Appl. Surf. Sci.*, 2014, **314**, 1000-1006.
61. C. Wang, X. Zhang, D. Zhang, C. Yao and Y. Ma, *Electrochim. Acta*, 2012, **63**, 220-227.
62. Y. Q. Wu, X. Y. Chen, P. T. Ji and Q. Q. Zhou, *Electrochim. Acta*, 2011, **56**, 7517-7522.
63. G. He, L. Wang, H. Chen, X. Sun and X. Wang, *Mater. Lett.*, 2013, **98**, 164-167.